3-D Active Shape Image Segmentation Using a Scale Model

Seong-Jae Lim and Yo-Sung Ho

Gwangju Institute of Science and Technology (GIST)
1 Oryong-dong, Buk-gu, 500-712, Gwangju, Korea

ABSTRACT

In this paper, we propose an active shape image segmentation method for three-dimensional (3-D) medical images. The approach consists of a generation method of a 3-D shape model and a segmentation method using a scale model. The 3-D shape generation method uses a tetrahedron algorithm for landmarking based on the view of geometry. After generating the 3-D model, we extend the shape model training and gray-level model training of two-dimensional (2-D) active shape models (ASMs). We use the integrated modeling process with scale and gray-level models for the appearance profile to represent local structure. Scale models are more compact, have more information in the region close to boundary, and have less information in the region far away from the boundary. Therefore, a scale can be considered as a weighting factor. Experimental results are comparable to those of manual tracing by the radiologist and 2-D ASMs, and demonstrate that this algorithm is effective for the semi-automatic segmentation method of livers.

Keywords : Active shape image segmentation, 3-D model generation, liver segmentation

1. INTRODUCTION

Biomedical images usually contain complex objects, which will vary in appearance significantly from one image to another. Attempting to measure or detect the presence of particular structures in such images can be a daunting task. The inherent variability will thwart naive schemes. However, it is possible to successfully analyses complex images by using models which can cope with the variability.

Active Shape Model (ASM) [1] algorithm usually performs well in many recognition tasks in two-dimensional (2-D) applications. They efficiently search images with a flexible and compact model by using prior knowledge derived from training data sets. It is possible to recognize objects with large variations in shape and appearance.

However, 2-D model-based ASMs do not provide a satisfying method for accurate segmentation in volume data. Also, it needs more than one model to use a 2-D model-based ASM in object data which has large shape variation.

Three-dimensional (3-D) model-based approaches are more promising than 2-D approaches since they can bring in more and realistic shape constraints for recognizing and delineating the object boundary. For 3-D model-based approaches, however, building the 3-D shape model from a training data set of segmented instances of an object is a major challenge and currently remains an open problem.

In building statistical shape models, one essential step is generally to generate a point distribution model (PDM). Corresponding landmarks must be selected in all training shapes for generating the PDM. In practice, correspondence has often been established using manually defined 'landmarks', but this is time-consuming, tedious, and error-prone. This is particularly true for 3-D approaches, where the amount of image data to analyze, and the number of landmarks required to describe the shape increase dramatically in comparison to 2-D applications [2].

Several methods for selecting landmarks in 2-D and 3-D have been proposed [3-5]. In Davies' method [3], correspondence is established by optimizing an information theoretic objective function based on the minimum description length approach. This method manipulates correspondence based on re-parameterising each training shape, showing the ability to build more compact models than the manual method. In Frangi's method [4], landmark selection is done by means of dense triangulations in a mean binary volume computed from the training set. Then, a free-form elastic registration technique based on maximization of normalized mutual information (volume-based technique) is used to propagate landmarks across the training shapes. The method of Hill [5] uses a direct approach to landmark selection by minimizing the total variance of a shape model. This requires an iterative local optimization scheme, and rebuilding the model at each stage. However, existing methods of PDM generation impose some constraints on the types of shapes that can be handled, and the resulting correspondences are essentially arbitrary.

In this paper, we propose a 3-D statistical shape model-based active shape image segmentation algorithm. For the 3-D active shape image segmentation algorithm, we use a generation method of 3-D statistical shape models proposed by Lim and Udupa [6]. Given a set of training 3-D shapes, 3-D model generation is achieved by 1) building the mean shape from the distance transform of the training shapes, 2) utilizing a tetrahedron method for automatically selecting landmarks on the mean shape, and 3) subsequently propagating these landmarks to each training shape via a distance labeling method. After obtaining the 3-D shape model, we perform a 3-D active shape image segmentation scheme by using scale and gray-level models for the appearance modeling. This combination model of a scale and a gray-level can bring in more accurate and precise results.

2. CONSTRUCTION OF 3-D SHAPE MODEL

In this section, we first present the required preliminaries from the previous works by Lim and Udupa [6]. Landmark finding is composed of three steps: creating the mean shape, landmark finding on the mean shape, and landmark propagation to other shapes. We assume that a set of 3-D binary images corresponding to the training shapes is given. These data sets are aligned and scaled via a 3-D affine transform first.

2.1. Mean Shape

After data alignment, all training data sets are in a common coordinate frame. Creating the mean shape is built by applying a distance transform $DT(b_i^{'})$ to each training shape $b_i^{'}$ that denotes the aligned shape, with the convention that the distances inside the boundary are negative and those outside are positive. Then, the mean of all distance transformed images is computed as follows [7] :

$$DT(b_m) = \frac{1}{n} \sum_{i=1}^{n} DT(b_i^{'}) \qquad (1)$$

This mean image is thresholded at 0 to get a binary image corresponding to a set of pixels whose distance value is at least 0 in the mean distance image. The digital boundary of this binary image (which represents the mean shape) is then found. Correspondence of landmarks on all training shapes is guided by the mean shape.

2.2. Landmark Finding

There are several methods for finding landmarks. All previous methods have some limitations of a shape. We propose a method for automatic landmarking from the view of geometry.

The proposed method is as follows :

(1) Find the major inertia axis of the surface S via PCA [8] and its points of intersection L_1, L_2 with S. Output points : L_1, L_2 .

(2) Find the farthest point L_3 on S from the line L_1L_2. If its distance from L_1L_2 is less than a fixed threshold θ, then stop. Else, output is L_3.

(3) Find the plane P containing L_1, L_2, L_3, and for one side of P, find the farthest point L_4 from P. If its distance from P is less than θ, then consider the other side of P and proceed recursively.

(4) Else output L_4, form new planes containing (L_1, L_2, L_4), (L_1, L_3, L_4), and (L_2, L_3, L_4) and proceed recursively.

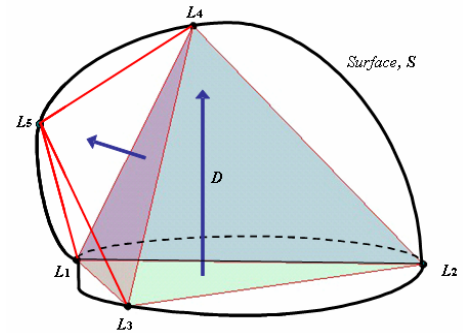*(5) Stop when no more planes need to be considered and no points are found with "distance to plane" greater than or equal to θ.*

Fig. 1. Tetrahedron method

Landmark threshold, θ is determined based on the degree of the compactness of a model that is its ability to describe the variability of a shape using as few modes as possible. The set of all output points by the procedure constitutes the set of landmarks defined for S. Figure 1 and Figure 2 illustrate the tetrahedron method and its block-diagram, respectively. In essence, the method recursively subdivides the interior of S into tetrahedra. When the method stops, it will have partitioned the interior of S into tetrahedra of various sizes whose union approximates the interior of S. The vertices of the tetrahedra constitute the landmarks on S.

When S is not convex, during recursive subdivision, there is no guarantee that the part of S on one side of the current dividing plane is connected. This is illustrated in Fig. 3 for the 2-D cases; both sides of L_1L_2 contain two connected components of S. In this case, therefore, connectivity analysis becomes necessary. Further, for each disconnected part (such as the concavity in the middle in Fig. 3), initial landmarks have to be found (in accordance with the first

step) to start the recursive process. This is done by finding the major inertia axis. That contour results from intersecting S with the plane, which is associated with the particular connected component. Subsequently the recursive process proceeds as previously described. When the above method is applied to the surface representing mean shape $\overline{S}$, we get a set L of labeled landmarks on $\overline{S}$.
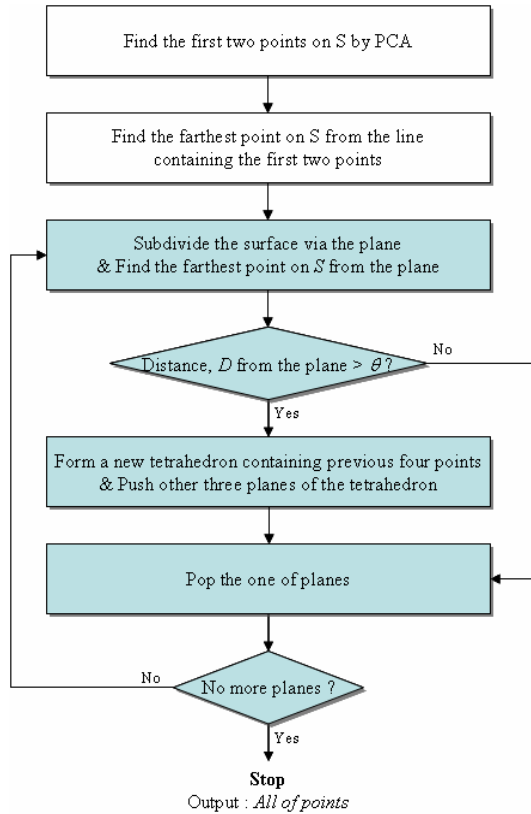

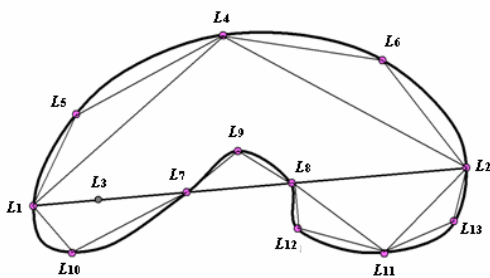Fig. 2. Block diagram of the tetrahedron method

Fig. 3. The illustration for a 2-D shape of the tetrahedron method

2.3. Landmark Propagation

For selecting corresponding landmarks L found on the surface of mean shape $\overline{S}$ in all training shapes, we propagate landmarks to each training shape. In this method, to propagate landmarks to the surface S of a given training shape, we use distance labeling to find the point on S that is closest to each landmark on $\overline{S}$. The distance value from each landmark of $\overline{S}$ is gradually increased. Whichever frontier (from a particular landmark) reaches a point of S first, determines the landmark label to be assigned to that point. In this manner, the points on S and their labels are determined simultaneously. This method again is very general and can be used in any dimensional space [6].

2.4. Creating the 3-D Shape Model

For creating the 3-D shape model, we use the ASM method to construct the statistical shape model from the information about landmarks on all training shapes. Principal component analysis (PCA) is applied to the aligned shape vectors. To this end, the mean shape $\overline{x}$, the covariance matrix S, and the eigensystem of S are computed. The eigenvectors p_i of S provide the modes of shape variation present in the data. The eigenvectors corresponding to the largest eigenvalue λ_i account for the largest variation; a small number of modes usually explain most of the variation. By sorting eigenvalues and corresponding eigenvectors in descending order, the t principal axes, or modes, responsible for a predefined level of variance, i.e. 95\% , can be identified. Let the specified quantile, q, be defined as

$$\sum_{i=1}^{t} \lambda_i \geq q \sum_{i=1}^{3n} \lambda_i \qquad (2)$$

3. ACTIVE SHAPE IMAGE SEGMENTATION

The training process for 3-D ASMs requires the extension of shape model training and gray-level model training. In addition to the training, the segmentation process must also be extended.

In the extension of shape model training, we use the 3-D statistical shape model of the previous section. However, the extension of gray-level models to 3-D requires a new profile sampling strategy. The gray-level models are formed by sampling all training volumes along the profile that is normal to the object surface. Once these profiles are extracted, the gray-level model for each landmark point consists of the objective function Eq. 3 where $\overline{g}$ and S_g are the mean profile and covariance matrix of all the profiles across the training set. The value of this function is the Mahalanobis distance between a candidate profile g_s and the mean profile $\overline{g}$.

$$f(g_s) = (g_s - \overline{g})^T S_g^{-1} (g_s - \overline{g}) \qquad (3)$$

There were two developments in the gray-level modeling process. Since the objects were landmarked after the reorientation process, the landmark points had to be mapped back to the original 3-D space before the gray-level profiles could be obtained. The second development was that of estimating the normals to the surface. The normal was taken as the mean of the normals to each triangle of the eight nearest neighbors in the surface.

We use the integrated modeling process with scale and gray-level models for the appearance model to represent local structure. The scale was previously proposed to determine the size of local structures at every pixel in the scene [9]. The scale at every pixel was defined as the radius of the largest ball centered at the pixel such that all pixels within the ball satisfied a predefined scene intensity homogeneity criterion. Similar with the gray-level appearance, the scale also can be used to build a morphometric appearance model to represent local structure. Compared with gray-level appearance models, scale models are more compact, have more information in the region close to boundary, and have less information in the region far away from the boundary. Therefore, the scale can be considered as a weighting image, giving the important part, such as interfaces, more weight. Eq. 4 is the weighing function of the integrated modeling process where f_s and α are the scale profile and the weighting factor, respectively. Figure 4 shows the example of scale models of a 2-D image and Fig. 5 illustrates the intensity along the profile on a scale model.

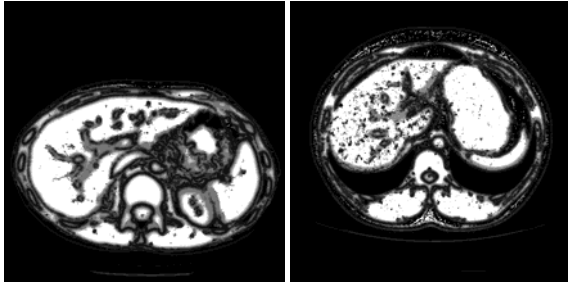$$f_o(g_s) = \alpha \cdot f_g(g_s) + (1-\alpha) \cdot f_s(g_s) \qquad (4)$$

Fig. 4. Scale models of 2-D CT image

After a shape model and combination (scale and gray)-level models are formulated, they work together to guide the process of searching for the surface of a new 3-D object within a volumetric data set. To implement the model deformation and search process, software was written to perform the following functions:

(1) *Given an initial location of 3-D landmark points within the new volume, update the position of all landmark points by minimizing the objective function (Eq. 4) .*

(2) *Adjust the set of landmark points to comply, in a statistical sense, with the shape model generated during training by adjusting the shape parameters in the PCA space.*

(3) *During segmentation, these two functions are called iteratively until the set of landmark points (i.e. shape) settles into a consistent position within the volume.*
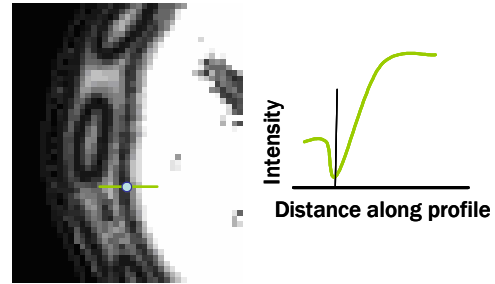

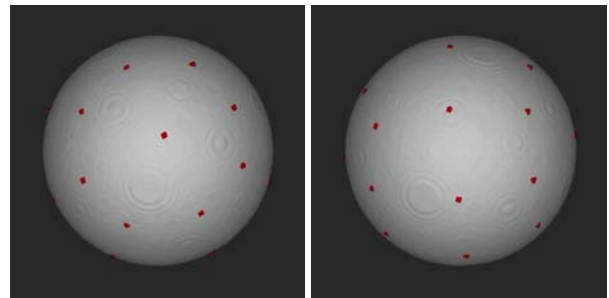Fig. 5. Intensity along profile on a scale model

4. EXPERIMENTAL RESULTS AND ANALYSIS

The image data sets used for validation were obtained from 30 standard CT liver scans of patients acquired in the venous phase of enhancement. Each CT image contains up to 71 image slices with an interslice spacing of 3.8mm.
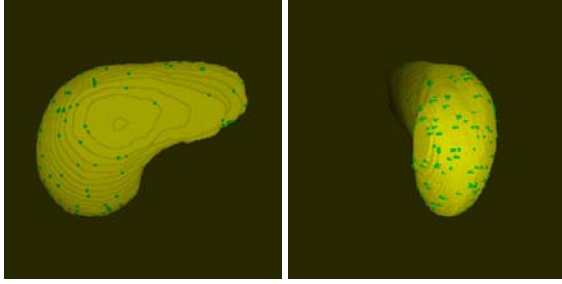
4.1. Evaluation of the 3-D Model Generation

Figure 5 (a) shows the example of a sphere whose radius is 50, and the landmark threshold of this example is 5. Figure 5 (b) shows the mean shape and landmarks on the mean shape of the liver. The number of landmarks is 170 and the surface size is 12757 voxels. The proposed method utilizing 170 landmarks captured 95\% shape variability with 3 modes. Recall that eigenvectors are axes along which the mean shape expresses variations.

In order to illustrate this fact, Fig. 6 displays the variations found in a given data set along the largest three principal axes.

(a) Landmarks on the sphere

(b) Landmarks on the liver

Fig. 5. Landmarks on the mean shape of 3-D shape

Figure 6 are converted landmarks to surface representation of the mean shape (middle) and the largest mode of variation for $b_1 = -3\sqrt{\lambda_1}$ (left) and $b_1 = 3\sqrt{\lambda_1}$ (right) via a convex hull algorithm. The modes are shown by displaying just the modified landmark positions with reference to the mean shape.

Fig. 6. Surface representation of landmarks via convex hull

The compactness of a model is its ability to describe the variability of a shape using as few modes as possible. In Fig. 7, we show the compactness, i.e., variance per mode, of the model generated by our method. The concentration of variability in the first m eigenvalues is shown in Fig. 7. It can be seen about 95\% of the shape variation is already captured by the first three eigenvectors.
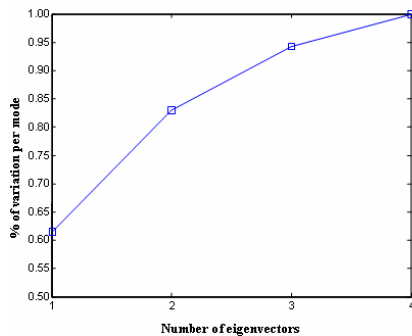

Fig. 7. Protion of variability captured by the first m eigenvectors

4.2. Evaluation of the 3-D ASM Algorithm

Figure 8 demonstrates the liver segmented manually by using the live-wire (LW) method in 3Dviewnix [11], a Unix-based software system for the visualization, manipulation, and analysis of multidimensional multi-parametric, multi-modality images. We use the manual segmentation result as truth for the accuracy measure. Figure 9 shows the liver segmented by using the proposed 3-D ASM method. We call the proposed 3-D ASM using a scale model *3-D ASM-s*.

For any scene, let C_o^b be the segmentation result (binary scene) output by the proposed method for which the true delineation result is C_t^b. The following measures, called false-positive volume fraction (*FPVF*) and true-positive volume fraction (*TPVF*) were used to assess the accuracy of the method [10].

$$TPVF(C_o^b, C_t^b) = \frac{|C_o^b \cap C_t^b|}{|C_t^b|} \times 100 \tag{5}$$

$$FPVF(C_o^b, C_t^b) = \frac{|C_o^b - C_t^b|}{|C_d - C_t^b|} \times 100 \tag{6}$$

where $|X|$ denotes the cardinality of set X. *TPVF* indicates the fraction of the total amount of tissue in the true delineation. *FPVF* denotes the amount of tissue falsely identified. C_d is a binary scene representation of a reference superset of voxels that is used to express the four measures as a fraction. We utilize *FPVF* and *TPVF* which are independent each other to describe accuracy. Table 1 lists the mean and standard deviation values of *FPVF* and *TPVF* achieved for the liver in CT images. Table 1 shows that the proposed 3-D ASM algorithm is more accuracy, efficiency and effective method than 2-D ASM algorithm.

Table 1. Mean and standard deviation of *FPVF* and *TPVF*.

	2-D ASM	3-D ASM	3-D ASM-s
FPVF	0.94 ± 0.03	0.96 ± 0.05	0.85 ± 0.06
TPVF	89.26 ± 1.52	90.67 ± 1.09	92.13 ± 1.04

5. CONCLUSIONS

We have described a method for three-dimensional (3-D) active shape image segmentation using a shape model. For the active shape image segmentation, we used a generation method of 3-D shape models previously proposed by us. The tetrahedron method for automatic landmark selection guided by the mean shape is independent of the object shape, geometry, and topology. The method can be used in any application for building 3-D models. For the segmentation, we proposed the integrated modeling process with a scale

model and a gray-level model for the appearance profile to represent local structure. Scale models are more compact, have more information in the region close to boundary, and have less information in the region far away from the boundary. Therefore, the combination of a scale modeling and a gray-level modeling can get more accurate and efficient results comparing with general active shape models (ASMs). The experimental results are comparable to those of manual tracing by the radiological doctor and 2-D ASMs, and demonstrate that this algorithm is effective more than 5% by comparison to 2-D ASMs and general 3-D ASMs.
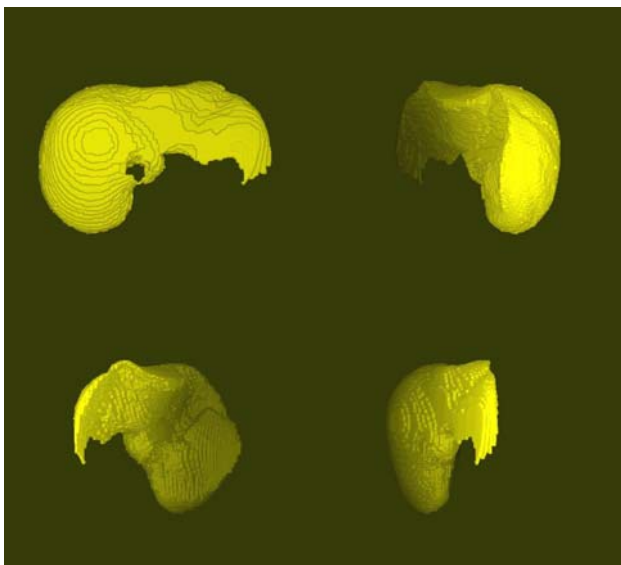

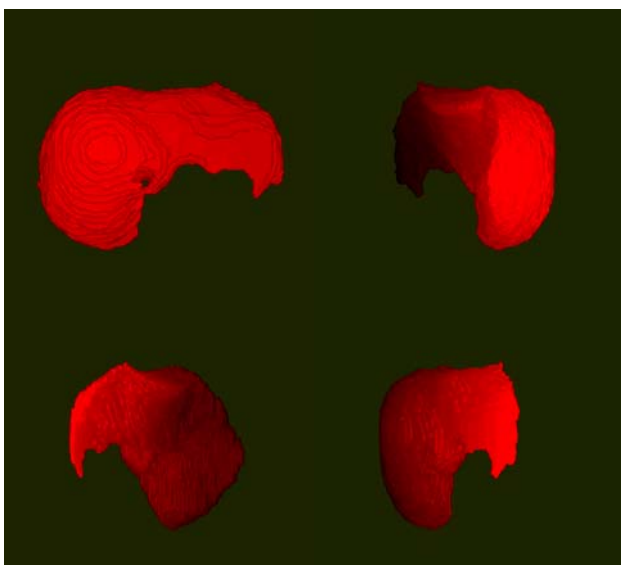Fig. 8. Liver segmented manually by using the LW method

Fig. 9. Liver segmented by using the 3-D ASM method

REFERENCES

[1] T.F. Cootes, D.J. Taylor, D.H. Cooper, and J. Braham, "Active shape models - their training and application," Computer Vision and Image Understanding, vol. 61, no. 1, pp. 38-59, 1995.

[2] A.F. Frangi, D. Rueckert, J.A. Schnabel, and W.J. Niessen, "Automatic Construction of Multiple-Object Three-Dimensional Statistical Shape Models: Applica-tion to Cardiac Modeling," IEEE Trans. Med. Imag., vol. 21, pp. 1151-1166, 2002.

[3] R.H. Davies, C.J. Twining, P.D. Daniel, T.F. Cootes, and C.J. Taylor, "Building optimal 2D statistical shape models," Image and Vision Computing, vol. 21, pp. 1171-1182, 2003.

[4] A.F. Frangi, D. Rueckert, J.A. Schnabel, and W.J. Niessen, "Automatic 3D ASM construction via atlas-based landmarking and volumetric elastic registration," Proc. of IPMI 2001}, vol. 2082, pp. 78-91, 2001.

[5] A. Hill and C.J. Taylor, "Automatic landmark generation for point distribution models," British Machine Vision Conference}, pp.429-438, 1994.

[6] S.J. Lim, J.K. Udupa, A. Souza, D. Torigian, Y.Y. Jeong, and Y.S. Ho, "A New, General Method of 3-D Model Generation for Active Shape Image Segmentation," Proc. of SPIE : Medical Imaging, vol. 4298, pp.48-55, 2006.

[7] A. Souza, and J.K. Udupa, "Automatic Landmark Selection for Active Shape Models," Proc. of SPIE : Medical Imaging, vol. 5747, pp. 1377-1383, 2005.

[8] E. Jackson, *A User's Guide to Principle Components*, Wiley & Sons, Inc., pp. 1-25, B.Jones 3-17-94, 1991.

[9] P.K. Saha, J.K. Udupa, and D. Odhner, "Scale-based Fuzzy Connected Image Segmentation : Theory, Algorithms, and Validation," Computer Vision and Image Understanding, vol. 77, pp. 145-174, 2000.

[10] J.K. Udupa, V.R. LaBlanc, H. Schmidt, C. Imielinska, P.K. Saha, G. Grevera, Y. Zhuge, L. Currie, P. Molholt and J. Yin, "Methodology for evaluating image seg-mentation algorithm," Proc. of SPIE : Medical Imaging, vol. 4684, pp. 266-277, 2002.

[11] J.K. Udupa, D. Odhner, S. Samarasekera, R. Goncalves, K. Iyer, K. Venugopal, and S. Furuie, "3D VIEWNIX: An Open, Transportable, Multidimensional, Multimodality, Multiparametric Imaging Software System," Proc. of SPIE, vol. 2164, pp. 58-73, 1994.